

# The Photoreactivity of Chlorine Dioxide

Veronica Vaida and John D. Simon

Determining the detailed photoreactivity of radicals that are of importance in atmospheric processes requires information from both laboratory and field measurements and theoretical calculations. Laboratory experiments and quantum calculations have been used to develop a comprehensive understanding of the photoreactivity of chlorine dioxide (OCIO). The photoreactivity is strongly dependent on the medium (gas phase, liquid solution, or cryogenic matrix). These data reveal details of the complex chemistry of OCIO. The potential role of this radical in stratospheric ozone depletion is discussed in accord with these laboratory measurements.

A significant effort has been made in recent years to elucidate the photoreactivity of polyatomic radicals. Advances in theoretical and experimental physical chemistry provide the tools needed to obtain detailed information on the molecular behavior of such complex systems. Modern spectroscopic techniques allow the mapping of reactive potential energy surfaces (PES's) and the unambiguous determination of reaction pathways, product yields, and their associated efficiencies. Advances in computational methodologies have made possible the generation of accurate ground-state and excited-state PES's for reactive small molecules. Understanding the effect of the medium on reactivity has provided a further challenge to experimental and theoretical chemists. Techniques currently used to bridge the understanding of reactivity from the gas phase to complex media include time-resolved studies in solution, reactions at surfaces, and molecular beam studies of van der Waals complexes. In this article we discuss the use of the complementary experimental and theoretical techniques mentioned above to study the photoreactivity of OCIO in gas and condensed phases. These findings are discussed in the context of the atmospheric chemistry of this radical.

The assessment of the role of OCIO in stratospheric processes has a long and interesting history. After the initial observations by Farman *et al.* (1) of the precipitous decline of Antarctic ozone ( $O_3$ ) at sunrise, the search for the molecular processes responsible prompted research into atmospheric measurement and modeling (2–4). Field measurements of the Antarctic stratosphere established a link between polar  $O_3$  loss and halocarbon chemistry (5–8); the increase of chlorine in the stratosphere correlated with the anthropogenic production of chlorofluorocarbons, Ground-based and air-

borne experiments discovered large enhancements of the concentrations of two oxides of chlorine, ClO and OCIO, in the stratosphere above Antarctica (2–8).

In addition to the catalytic reaction with  $O_3$  (9), Cl reacts with other trace gases in the stratosphere to form HCl and ClONO<sub>2</sub>. These molecules do not undergo reaction in the gas phase and therefore provide reservoirs for chlorine. It is not possible to account for the huge Antarctic  $O_3$  losses without including reactions that occur on the surfaces of cloud particles (10–14). On the surfaces of polar stratospheric clouds (PSC's), HCl and ClONO<sub>2</sub> react to release active Cl and keep the stratospheric reactive Cl concentrations very high (10–14). Consequently, in accounting for the chemistry of the  $O_3$  hole, research has focused on both homogeneous (gas phase) and heterogeneous (aerosol) catalytic cycles involving oxides of chlorine.

Although a complete discussion of  $O_3$  depletion is outside the scope of this report, laboratory studies of the photochemistry of chlorine oxides generally agree that photolysis of the ClO dimer is the dominant chemical reaction responsible for Antarctic  $O_3$  loss (15, 16). The coupling of chlorine and bromine chemistry (reaction of ClO and BrO) to form the thermally unstable, asymmetric isomer ClOO (and Br) is another important  $O_3$  loss pathway (17). The ClOO molecule fragments into Cl atoms and  $O_2$ .

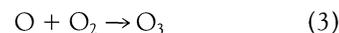
The importance of these different chemical processes to  $O_3$  depletion depends on geographical concerns. For example, the higher winter temperature in the Arctic relative to the Antarctic precludes PSC formation. Consequently, in the Arctic there are lower chlorine concentrations, lower ClO concentrations, and as the ClO dimer concentration scale with the square of the ClO concentration, significantly lower ClO dimer concentrations. In this region of the globe, it is possible that the coupling of chlorine and bromine chemistry (ClO + BrO reactions) plays a more impor-

tant role than other processes (3). Current restrictions that still allow some use of chlorine and the lack of regulations on bromine suggest that one can expect an increasing impact of this chemistry on stratospheric processes.

We now consider the reaction of ClO and BrO (17) which in addition to forming ClOO as mentioned above, also forms the symmetric isomer OCIO (18)



This reaction is the only established chemical process in the stratosphere that generates OCIO. Laboratory results indicate that the photochemical decomposition of ClClO<sub>2</sub> also generates OCIO (19), but the reactivity and role of ClClO<sub>2</sub> in the atmosphere remain to be determined. The relative yields for the formation of ClOO and OCIO from the reaction of ClO and BrO are temperature-dependent, and the symmetric isomer is preferentially formed below 250 K (18). Until recently (20), OCIO was thought to play no role in  $O_3$  loss chemistry, although it is present in high concentrations. The gas-phase photochemistry was thought to only involve formation of O atoms, which would subsequently react with  $O_2$  to reform  $O_3$



(The photon energy is given by Planck's constant  $h$  multiplied by the frequency of the light  $\nu$ .) Thus, formation and destruction of OCIO would not result in any net loss of  $O_3$ .

In the remainder of this article, we focus on the current understanding of the reactivity of OCIO. The results from gas phase, liquid solution, matrix spectroscopy, and photochemical studies are combined with theoretical calculations of the ground-state and excited-state PES's to provide an unambiguous identification of new photoreactive channels of OCIO. Several of these suggest new mechanisms by which OCIO can cause  $O_3$  loss chemistry in the stratosphere.

## Thermal Reactivity of Chlorine Dioxide

The available information on the ground-state reactivity of OCIO is given as part of the correlation diagram in Fig. 1. The electronic ground state of OCIO lies  $\sim 4$  kcal/mol above that of the ClOO isomer (21). Spectroscopic data and theoretical calcula-

V. Vaida is in the Department of Chemistry and Biochemistry, University of Colorado, Boulder, CO 80309, USA. J. D. Simon is in the Department of Chemistry and Biochemistry, University of California at San Diego, La Jolla, CA 92093-0341, USA.

tions provide information on the equilibrium structures and the frequencies of the vibrational normal modes for both isomers. Although ClOO is thermodynamically more stable than OClO, ClOO is kinetically unstable and dissociates into Cl and O<sub>2</sub> (22). Most of the relevant information on ClOO has been derived from electron spin resonance and infrared (IR) experiments in matrices (23, 24) and ultrafast measurements in solution (25–29). In good agreement with experiment, calculations by Peterson and Werner (21) suggest a geometry in which the Cl–O and O–O bond lengths are 2.139 and 1.291 Å, respectively, and the bond angle is 115.7°; the O–O bond length is nearly that of free O<sub>2</sub> (1.207 Å).

Because of its kinetic stability, OClO has been the subject of detailed experimental studies. The ground-state geometry is a near prolate asymmetric top with a bond length  $r_e(\text{ClO}) = 1.47 \text{ \AA}$  and a bond angle of 117.4°. Experimental data yield the following ground-state fundamental vibrational frequencies (30, 31):  $\nu_1 = 946 \text{ cm}^{-1}$  (symmetric stretch),  $\nu_2 = 448 \text{ cm}^{-1}$  (bend), and  $\nu_3 = 1110 \text{ cm}^{-1}$  (asymmetric stretch). The energies are in excellent agreement with theory (21); however, the experimentally observed IR intensities for these normal modes cannot be quantitatively explained. The discrepancy between theoretical and experimental intensities is best explained in terms of the ground-state dynamics. The spectral lines corresponding to reactive modes are characterized by large linewidths and diminished peak intensities. Spectroscopic studies of the overtone and combination transitions of isotopically labeled molecules (O<sup>35</sup>ClO and O<sup>37</sup>ClO) have focused on the ground-state potential away from equilibrium. However, the part of the potential that can be probed in this fashion does not include the energy region relevant to reaction. For the energy region studied, the intensities of overtones ( $2\nu_2$ ) and combinations ( $\nu_1 + \nu_2$ ,  $\nu_1 + \nu_2 + \nu_3$ ) containing the bending mode are low compared to the intensities of transitions involving the same number of quanta of the symmetric ( $2\nu_1$ ) and asymmetric stretch ( $\nu_1 + \nu_3$ ,  $2\nu_1 + \nu_3$ ). The intensities of the  $\nu_1$  and  $\nu_2$  fundamentals are nearly the same. A harmonic approximation for the PES's predicts that the combinations and overtones of these modes should also have nearly equal intensities. The observed small intensities of bending modes can be attributed to large linewidths caused by short lifetimes. This result suggests the involvement of the bending mode in promoting the ground-state reactions of OClO.

A kinetic study of the thermal decomposition of OClO initiated by a shock wave revealed an activation energy for reaction

of  $\sim 15 \text{ kcal/mol}$  (32). The experimental observations suggest a collisionally induced dissociation of OClO into  $\text{Cl}(^2P_u) + \text{O}_2(^3\Sigma_g^-)$ . The spectroscopic and kinetic data (30–32) suggest that bending promotes dissociation to Cl and O<sub>2</sub> on the ground-state PES. Two possible reaction coordinates can be followed during the reaction. First, the reaction may proceed by a symmetrical process in which a C<sub>2v</sub> symmetry is preserved throughout the reaction. Second, the reaction may proceed asymmetrically, with the possible involvement of ClOO as a reaction intermediate. Matrix isolation experiments (23, 24) and theoretical calculations (21) suggest that isomerization of OClO to ClOO has a lower activation energy than the symmetric dissociation to Cl and O<sub>2</sub>. These data argue that the 15-kcal/mol barrier observed in the kinetic measurements (32) corresponds to the activation energy needed for the OClO–ClOO isomerization reaction. Vaida *et al.* determined (26) that the barrier height for this reaction in water solution is 12 kcal/mol, slightly lower than the value measured in the gas-phase reaction.

### Photoreactivity of Chlorine Dioxide

Excitation of OClO in the near-ultraviolet (near-UV) accesses a set of coupled PES's on which reaction occurs efficiently. Photoreactivity from this complex manifold of states is susceptible to intermolecular interactions and leads to significant differences between the gas-phase photoreactivity and the photoreactivity observed in condensed-

phase environments such as liquid solutions and solid matrices. We examined those differences in photoreactivity in an effort to develop a unified model for the photoreactions of OClO.

**Symmetry considerations.** In the energy range relevant to atmospheric photochemistry, there are three closely spaced electronic states. The adiabatic electronic-state correlations for two symmetry cases (C<sub>2v</sub> and C<sub>s</sub>) are considered in Fig. 1. The C<sub>2</sub> axis is taken to be the z axis, and the x axis is defined to be perpendicular to the plane of the molecule.

In C<sub>2v</sub> symmetry, the combination of ground-state chlorine,  $\text{Cl}(^2P_u)$ , and ground-state oxygen,  $\text{O}_2(^3\Sigma_g^-)$ , correlates to the ground  $^2B_1$  and the excited  $^2A_1$  and  $^2A_2$  electronic states. Energetic considerations suggest that O<sub>2</sub> can be generated in several different electronic states ( $^3\Sigma_g^-$ ,  $^1\Delta_g$ ,  $^1\Sigma_u^+$ ). The combination of ground-state chlorine  $\text{Cl}(^2P_u)$  and excited-state oxygen  $\text{O}_2(^1\Delta_g)$  correlates to the first electronic excited state of OClO of  $^2B_2$  symmetry, among several others. All three of these excited doublet states ( $^2A_2$ ,  $^2A_1$ , and  $^2B_2$ ) correlate with dissociation into  $\text{ClO}(^2\Pi) + \text{O}(^3P)$ .

In C<sub>s</sub> symmetry, the same combination,  $\text{Cl}(^2P_u) + \text{O}_2(^3\Sigma_g^-)$ , correlates to three electronic states of OClO: two of  $^2A''$  symmetry and one of  $^2A'$  symmetry. The first  $^2A''$  state correlates to the ground states of ClOO and OClO. The  $^2A'$  state correlates with a low-lying excited state of ClOO and to the first excited state of OClO ( $^2B_2$  in C<sub>2v</sub>). The second  $^2A''$  state correlates to a higher excited state of ClOO and to the third excited state of OClO ( $^2A_2$  in C<sub>2v</sub>).

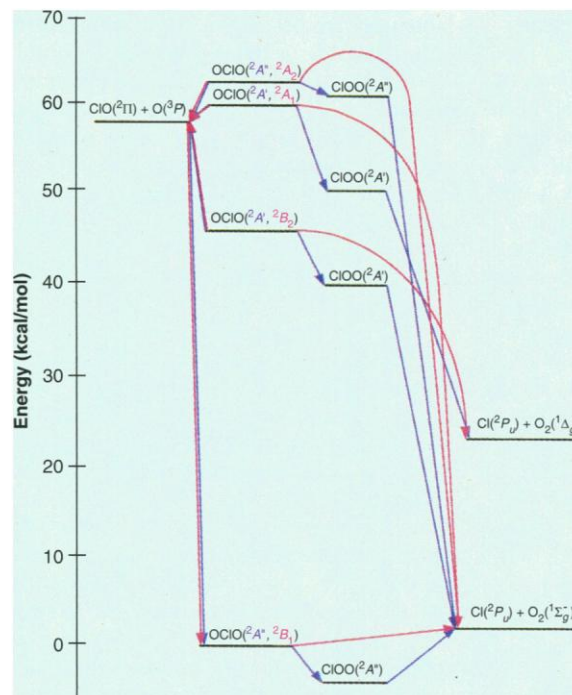


**Fig. 1.** Orbital correlation diagrams for the reactivity of OClO assuming a C<sub>s</sub> (blue) and C<sub>2v</sub> (red) reaction coordinate. State energies are calculated (21) equilibrium values.

The combination of  $\text{Cl}(^2P_u) + \text{O}_2(^1\Delta_g)$  gives rise to three  $^2A'$  states and three  $^2A''$  states. One of these  $^2A'$  states correlates with the second  $^2A'$  excited state in ClOO and with the second excited state in ClOO (formerly  $^2A_1$  in  $C_{2v}$ ). All of these states (two  $^2A'$  and two  $^2A''$  states) correlate to  $\text{ClO}(^2\Pi) + \text{O}(^3P_g)$  products. Calculations predict that all doublet excited states of ClOO are repulsive along the Cl–O<sub>2</sub> coordinate. Only the ground  $^2A''$  state is bound along this coordinate. On the basis of extensive calculations (21, 33, 34), the two  $^2A'$  and one  $^2A''$  excited states of ClOO are positioned at 44, 55, and 65 kcal/mol, respectively, well above the ClOO ground-state level. These states are nearly isoenergetic with the doublet excited states of OCIO. Coupling between the excited states of ClOO and OCIO needs to be considered in discussing excited-state reactivity.

These symmetry considerations make it possible for us to identify possible reactions. Correlation diagrams do not provide information on the detailed reaction coordinate; the photoreactive pathways shown in Fig. 1 may not actually occur because of internal conversion (from the  $^2A_2$  state to lower energy excited states) or the presence of a potential barrier along a particular reaction coordinate for an electronic state that can decompose by several competing pathways. These issues can, however, be addressed

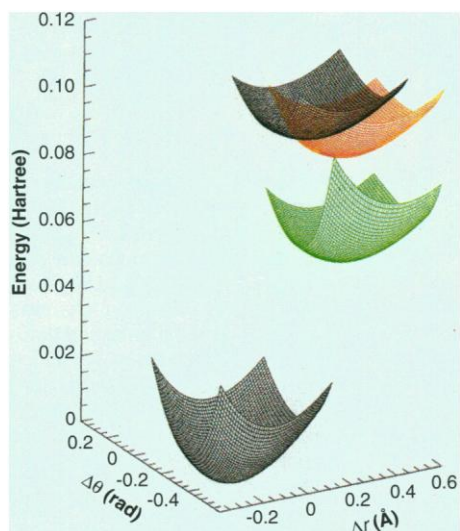


**Fig. 2.** Calculated (21) near-equilibrium PES's for the ground ( $^2B_1$ ; black) and for the lowest three excited states of OCIO ( $^2A_2$ ; black,  $^2A_1$ ; orange,  $^2B_2$ ; green). The energy for each state is plotted as a function of the change in the symmetric bond length  $\Delta r$ , and the bond angle  $\Delta\theta$  relative to the equilibrium structure of the ground electronic state. The excited states are significantly displaced from the ground-state structure. However, the PES's are closely spaced within the Franck-Condon region. A total energy spacing among the three states is estimated to be on the order of 12 kcal/mol.

through experimental measurements of the photofragment internal energies and ab initio calculations of PES's and reaction paths.

*Gas-phase photochemistry.* Figure 2 shows the symmetric part of the PES's calculated by Peterson and Werner (21) for the near-equilibrium geometry of OCIO in the  $^2A_2$  (black),  $^2A_1$  (orange), and  $^2B_2$  (green) states. The axes reflect the change in bond angle ( $\Delta\theta$ , in radians) and in the symmetric bond length ( $\Delta r$ , in angstroms) relative to the equilibrium structure in the ground state. Clearly, the minima of these states indicate different bond lengths and angles, which can affect reactivity. Electronic dipole selection rules predict that the  $^2B_2 \leftarrow ^2B_1$  transition is forbidden; the  $^2A_1 \leftarrow ^2B_1$  transition is allowed but is of perpendicular polarization (weak); the  $^2A_2 \leftarrow ^2B_1$  transition is allowed and is of parallel polarization (strong). Spectroscopic experiments detect excitation only to the  $^2A_2$  state.

The symmetric part of the potential determined on the basis of the spectroscopic information (35, 36) is shown in Fig. 3. The vertical band drawn in Fig. 3 indicates the part of the potential that is accessed by absorption spectroscopy (the Franck-Condon region). The corresponding spectrum (shown along the y axis) consists of intense and long progressions in the symmetric stretch ( $\nu_1$ ) and combinations of the bend ( $\nu_2$ ) and even quanta of the asymmetric stretch ( $\nu_3$ ) built on  $\nu_1$ . All of these bands show isotopic shifts reflecting the presence of both  $\text{O}^{35}\text{ClO}$  and  $\text{O}^{37}\text{ClO}$ . Analysis of the bands (energy, intensity, and isotopic shifts) obtained from high-resolution rovi-

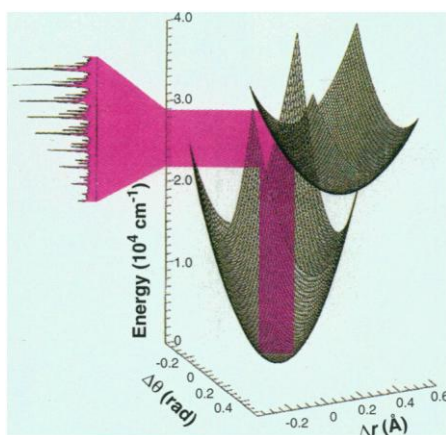


**Fig. 3.** Spectroscopically obtained PES's for OCIO (35, 36) for the  $^2B_1$  ground and  $^2A_2$  excited states of OCIO plotted as a function of the change in the symmetric bond length  $\Delta r$ , and the bond angle  $\Delta\theta$  relative to the equilibrium structure of the ground electronic state. The pink band indicates the Franck-Condon region associated with the symmetry-allowed  $^2A_2 \leftarrow ^2B_1$  transition. The corresponding absorption spectrum is given along the y axis.

brational spectra provides insight into the molecular structure on this excited PES (35–38). These data are consistent with a decrease in bond angle ( $117^\circ$  to  $107^\circ$ ) and an increase in Cl–O bond length (1.47 to 1.63 Å) associated with excitation to the  $^2A_2$  state. High-resolution jet-cooled spectra have made it possible to determine the excited-state structure of OCIO along all normal coordinates. The optical spectrum suggests that all modes are active in transitions to the excited state, and therefore all can play a role in the near-UV photochemistry.

The high-resolution jet-cooled spectra could also be exploited to give dynamical information (36). In particular, the natural linewidths of the rovibronic transition provide important insights into mode-specific excited-state lifetimes. Transitions to the  $^2A_2$  excited state exhibit lifetimes ranging from 20 ps to 200 fs. The lifetime is independent of the particular rotational level excited for a given vibrational mode, but there is a strong vibrational dependence on the dynamics. The large linewidths for combinations of  $\nu_2$  and  $\nu_3$  indicate short lifetimes. Thus, the bend and the asymmetric stretch facilitate reaction. In combination with the theoretical calculations of Peterson and Werner (21), these data show that the asymmetric stretch accesses the reaction channel that forms ClO + O, whereas the bend enhances production of Cl + O<sub>2</sub>.

Zewail's group (39) recently measured the corresponding time scale for decay into these two channels to be 200 and 60 fs, respectively. Photofragmentation studies (40–44) detected the products  $\text{ClO}(^2\Pi) + \text{O}(^3P)$  and  $\text{Cl}(^2P_u) + \text{O}_2(^3\Sigma_g^-, ^1\Delta_g)$ , which supports the conclusion that both reaction channels occur. The nascent ClO fragment has been shown (40) to be rotationally cool and vibrationally excited, with the real distribution remaining to be determined. Recent experimental work clearly establishes that the two reaction channels are mode-specific. Bishenden and Donaldson (41) reported that excitation of the asymmetric stretch enhances the production of ClO over that of Cl. This point had been conjectured on the basis of spectroscopic information (35, 36) and theoretical calculations (21, 33, 34). Davis and Lee (42) found that excitations of the bend enhances O<sub>2</sub> production. These studies highlight the complexity of the excited-state dynamics that can arise from the nested manifold of excited states.

Understanding OCIO photoreactivity requires multidimensional calculations like those reported by Peterson and Werner (21). The experimental observations (35, 36, 40–44) are in excellent accord with the theoretical predictions of Peterson and Werner (21, 33, 34). Mechanisms consis-

ment with product distributions and molecular symmetries need to be proposed to account for these observations. The proposed reaction mechanisms are sketched in Fig. 4. Excitation to the  ${}^2A_2$  state is followed by internal conversion to the  ${}^2A_1$  state through spin-orbit coupling. This state accesses allowed reaction pathways that form  $\text{ClO}({}^2\Pi) + \text{O}({}^3P)$  and  $\text{Cl}({}^2P) + \text{O}_2({}^1\Delta_g, {}^3\Sigma_g^-)$ . Vibronic coupling can also result in internal conversion from the  ${}^2A_1$  state to the reactive  ${}^2B_2$  state. Here, the reaction channels mentioned are open as well as isomerization to form CIOO. At the present time, the quantum yields for different reaction channels are still controversial. The model we present suggests that photochemical quantum yields will be wavelength-dependent. Once these wavelength-dependent quantum yields are obtained experimentally, the rate constant ( $J$  values) can be determined and the quantitative impact of OCIO on atmospheric processes can be assessed. Theoretical calculations reveal barriers to reaction from the  ${}^2A_1$  state, which has led to the current view that all photoreactivity of OCIO emanates from the  ${}^2B_2$  state (21, 33, 34).

The above discussion demonstrates how modern physical chemistry techniques can be used to provide detailed information about the photoreactions of small molecules. With the discovery of reaction channels leading to Cl production, it is clear that the photoreactivity of OCIO can impact the current understanding of stratospheric photocycles. Recently, there has been considerable interest in elucidating the role of heterogeneous catalysis reactions of chlorine oxides. Toward this end, it is important to examine how the effects of the medium alter the molecular photoreactivity of OCIO.

**Solution photochemistry.** The photochemistry of OCIO in solution has recently been studied in detail (25–29, 45, 46). Here, we focus on the reactivity of OCIO in water and sulfuric acid ( $\text{H}_2\text{SO}_4$ ) solutions. In water, OCIO photochemically reacts to form  $\text{HCl}$  and  $\text{HClO}_3$ ; the reaction products in  $\text{H}_2\text{SO}_4$  are not known. Solvation broadens the sharp spectral features observed in the gas-phase  ${}^2B_1 \leftarrow {}^2A_2$  absorption band, thereby precluding any detailed information on the electronically excited molecular structure and dynamics from a spectroscopic analysis. In solution, vibrational relaxation and internal conversion in the excited-state manifold generally occur on time scales more rapid than photoreactions. Thus, one expects that all of the observed solution chemistry will occur from the  ${}^2B_2$  excited state.

In accord with this expectation, and in contrast to the case of the isolated molecule, the chemistry observed in solution is independent of excitation wavelength. Pi-

cosecond time-resolved spectroscopic studies of the photoreactivity of OCIO in water reveal that 90% of the excited molecules fragment into  $\text{OCl} + \text{O}$  with the remaining 10% generating  $\text{Cl} + \text{O}_2$  (28). Examination of the orbital correlations given in Fig. 1 shows that Cl can be formed by two distinct mechanisms: (i) direct elimination of Cl from OCIO, maintaining the  $C_{2v}$  symmetry axis along the reaction coordinate to form  $\text{Cl} + \text{O}_2({}^1\Delta_g)$ ; and (ii) isomerization to CIOO, which thermally dissociates into  $\text{Cl} + \text{O}_2$ . In the gas phase, the identification of  $\text{O}_2({}^1\Delta_g)$  is a challenging experiment. The time-of-flight data in the photofragmentation experiments of Davis and Lee (42) suggests that this channel is open. In solution,  $\text{O}_2({}^1\Delta_g)$  can be directly quantified by measuring the intensity of the  $\text{O}_2$  emission ( ${}^3\Sigma_g^- \leftarrow {}^1\Delta_g$ ) relative to known standards. The emission quantum yield after excitation of OCIO in water shows that the direct elimination of Cl constitutes 5% of the total Cl generation (29). The remaining Cl forms from the thermal decomposition of CIOO. In turn, CIOO is formed within the time resolution of the experiment, probably through excited-state isomerization of OCIO. These data unequivocally show that Cl is produced by two competitive pathways. The quantum yield for  $\text{Cl} + \text{O}_2({}^1\Delta_g)$  production is solvent-dependent, increasing in efficiency as the dielectric constant of the solvent decreases.

The CIOO produced from photoexcited OCIO “lives” for about 1 ns in water solution (27, 28). This long lifetime makes it possible to investigate the solution spectroscopy of this reactive molecule. Such data

can be useful in the structural characterization of this radical (CIOO is difficult to study in the gas phase because of its kinetic instability). Theoretical calculations suggest the existence of low-lying excited electronic states that would give rise to absorption spectra in the visible region of the spectrum (33, 34). However, for gas-phase samples, only a UV transition has been reported. In many of the solvents studied, an absorption feature in the visible part of the spectrum has been observed that exhibits kinetics identical to those of the known UV absorption band of CIOO (27). These observations provide compelling evidence that CIOO has one or more electronic excited states similar in energy to the lowest energy states of OCIO.

The observed reactivity of OCIO in  $\text{H}_2\text{SO}_4$  is similar to that observed in water. Dissociation into both  $\text{ClO} + \text{O}$  and  $\text{Cl} + \text{O}_2$  are observed; oxygen  ${}^3\Sigma_g^- \leftarrow {}^1\Delta_g$  emission is also detected (27, 29). Unfortunately, it is not currently possible to quantify the efficiencies of these reaction channels as standards for neat  $\text{H}_2\text{SO}_4$  solutions are not known. These data, however, serve as important reference points for results obtained in  $\text{H}_2\text{SO}_4$  matrices.

**Matrix photochemistry.** Matrix spectra of OCIO also exhibit significant broadening compared to the gas-phase spectrum (23, 24, 47, 48). This broadening most likely results from the heterogeneity of the sites occupied by OCIO. Thus, matrices, like solutions, preclude obtaining geometric information about electronically excited states of OCIO from a spectroscopic analysis. Photolysis studies (23, 24, 47, 48) of OCIO in

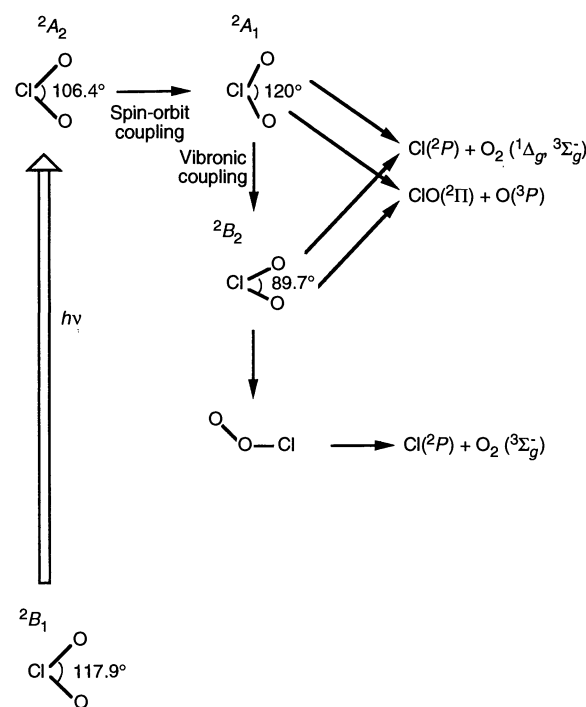
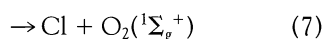
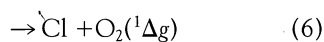
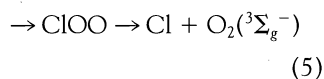
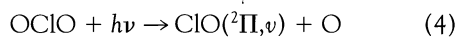


**Fig. 4.** Schematic representation of the photoreactivity of OCIO. Excitation directly populates the  ${}^2A_2$  state. Spin-orbit coupling causes a surface crossing to the  ${}^2A_1$  state from which multiple reaction channels can occur. Experimental and theoretical results suggest that the dominant pathway is internal conversion to the  ${}^2B_2$  state through vibronic coupling. Once the  ${}^2B_2$  state is populated, three reactions compete: bond cleavage giving  $\text{ClO} + \text{O}$ , elimination forming  $\text{Cl} + \text{O}_2$ , and isomerization to CIOO, which then generates  $\text{Cl} + \text{O}_2$ .

matrices have reported quantitative formation of ClOO when the photolysis wavelength is near the maximum of the near-UV transition (360 nm). Recent results (47, 48) suggest that, in the matrix, OCIO may dissociate to form Cl and O<sub>2</sub>, which then recombine to form ClOO. If this is the case, there would be a substantial change in the quantum efficiency for this process in the matrix as compared to that in the gas phase. Thus, the behavior of OCIO in cold matrices is significantly different from that observed in the gas phase and in room-temperature solution.

### A Unified Photochemical Model

From a combination of gas phase, solution, and matrix isolation experiments, we conclude that electronically excited OCIO undergoes four competitive reactions:



(The  $\nu$  in Eq. 4 indicates that the product consists of a distribution between ground and excited vibrational levels). The partitioning in these pathways depends on the molecule's environment. These effects can be understood in terms of the accessible electronic surfaces, general mechanism, and correlation diagram shown in Figs. 1 and 4. In addition, comparison of the data obtained in different environments suggests processes that may occur in the atmosphere.

The quantum yield for total Cl production from photoexcited OCIO deserves special attention, as it is this channel that will have a major impact on the relevance of OCIO to atmospheric concerns. In the gas phase, in water solution, and in a low-temperature matrix, the quantum efficiency for Cl generation is <0.1 (mode-specific), 0.1, and 1.0, respectively. The effect of solvation on the energetics of the allowed photochemical pathways should be considered. In the gas phase, in solution, and in matrices, photoisomerization to ClOO and direct C<sub>2v</sub> dissociation to Cl(<sup>2</sup>P<sub>u</sub>) + O<sub>2</sub>(<sup>1</sup>Δ<sub>g</sub>) are highly exothermic reactions. Solvation effects will only increase the exothermicity of channels that create atomic Cl (through the formation of a Cl-solvent donor-acceptor complex) and have a negligible effect on the isomerization reaction (27).

However, this is not the case for the asymmetric ClO + O dissociation reaction. The ground-state OCIO → ClO(<sup>2</sup>Π) + O(<sup>3</sup>P<sub>g</sub>) dissociation reaction is endothermic by 58 ± 2 kcal/mol. The calculations of

Peterson and Werner (21) indicate that the <sup>2</sup>B<sub>2</sub> excited state, from which dissociation occurs, is only slightly higher in energy, 2 to 3 kcal/mol, than the ClO(<sup>2</sup>Π) + O(<sup>3</sup>P<sub>g</sub>) products. A small barrier, on the order of *k<sub>B</sub>T* (where *k<sub>B</sub>* is the Boltzmann constant and *T* is temperature), is calculated. Given this small energy difference, solvent effects on the energetics of this reaction can dramatically affect the ability of this reaction channel to compete with both isomerization to ClOO and direct dissociation to Cl(<sup>2</sup>P<sub>u</sub>) + O<sub>2</sub>(<sup>1</sup>Δ<sub>g</sub>).

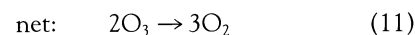
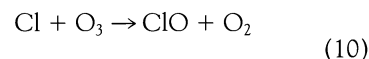
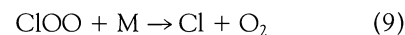
The difference in solvation free energies, Δ(Δ*G*), for ClO + O and OCIO(<sup>2</sup>B<sub>2</sub>) can be estimated with dielectric continuum models for the liquid (49). Here, Δ(Δ*G*) depends on the ratio of the square of the dipole moment to the molecular volume. The dipole moments of ClO and OCIO(<sup>2</sup>B<sub>2</sub>) are 1.2 and 2.46 D, respectively. The energy of the <sup>2</sup>B<sub>2</sub> state of OCIO will be more sensitive to the solvent than the ClO fragment. This approach estimates that water stabilizes OCIO(<sup>2</sup>B<sub>2</sub>) by 2.8 kcal/mol more than it does the dissociation products. In liquid argon at -191 K, Δ(Δ*G*) is estimated to be 0.74 kcal/mol, still significant compared to thermal energy.

Combining this information with the ab initio calculations suggests that solvation in both liquids and matrices could make this reaction channel isoenergetic to slightly endothermic. If this reaction barrier were on the order of *k<sub>B</sub>T* in room-temperature solution, it could be as much as 4 *k<sub>B</sub>T* at 77 K, making this channel energetically inaccessible from the <sup>2</sup>B<sub>2</sub> excited state for OCIO in low-temperature matrices. Such an effect could easily account for differences in the quantum efficiency for Cl + O<sub>2</sub> formation observed between liquid and matrix H<sub>2</sub>SO<sub>4</sub>. (In liquid H<sub>2</sub>SO<sub>4</sub>, photolysis of OCIO generates transient species consistent with the ClO + O channel and <sup>3</sup>Σ<sub>g</sub><sup>-</sup> ← <sup>1</sup>Δ<sub>g</sub> emission is observed from the O<sub>2</sub> fragment, indicating that Cl + O<sub>2</sub> is also produced, whereas only isomerization to ClOO is observed in the matrix.) On the basis of these observations, it is interesting to ask whether in matrices there is a partitioning at low temperature between direct dissociation to Cl + O<sub>2</sub>, followed by cage recombination to form ClOO and isomerization to ClOO. Experimental measurements should be able to address the relative importance of these channels as direct dissociation produces O<sub>2</sub>(<sup>1</sup>Δ<sub>g</sub>). As Cl(<sup>2</sup>P<sub>u</sub>) + O<sub>2</sub>(<sup>1</sup>Δ<sub>g</sub>) does not correlate with any of the accessible states of ClOO, O<sub>2</sub> must electronically relax before reacting. The resulting <sup>3</sup>Σ<sub>g</sub><sup>-</sup> ← <sup>1</sup>Δ<sub>g</sub> emission may be observable in the matrix, and a determination of the quantum yield could further substantiate the unification between the liquid and matrix photochemistry.

### A Reevaluation of OCIO in Stratospheric Processes

The elucidation of the photoreactivity of OCIO implicates this molecule in O<sub>3</sub> depletion. The discovery of a reaction path to Cl and O<sub>2</sub> directly couples the photochemistry of OCIO to O<sub>3</sub> loss (20). The importance of this process to overall stratospheric O<sub>3</sub> depletion depends on the quantum yield for Cl generation, a number that is still controversial (40–44), ranging up to 10% in gas phase. The wavelength-dependent quantum yields have yet to be measured accurately; however, if the quantum yield over the entire absorption spectrum were 10%, a total Antarctic O<sub>3</sub> loss of ~3% is predicted. The full effect of OCIO photochemistry on stratospheric O<sub>3</sub> concentrations requires measurement of the wavelength-dependent product branching ratios and quantum yields, from which the rate constants (*J* values) can be determined for subsequent inclusion in atmospheric models.

The observed photoreactivity of OCIO suggests the possibility of additional contributions to O<sub>3</sub> depletion that are unexplored. The major photoproduct of the near-UV photolysis of OCIO is vibrationally excited chlorine oxide, ClO(<sup>2</sup>Π,  $\nu$ ). The reactivity of this energized intermediate is not known. Further study of reaction rates with other molecular species and of vibrational quenching rates is needed. Anderson and co-workers (50, 51) have investigated the ClO catalytic depletion of O<sub>3</sub> by the following mechanism



The measured rate constant for Eq. 8 suggested negligible loss arising from the above cycle. However, Ruhl *et al.* (40) showed that photolysis of OCIO generates ClO(<sup>2</sup>Π,  $\nu$ ) with internal energy in excess of the reaction barrier with O<sub>3</sub>. To estimate the rate of loss of O<sub>3</sub> from reaction with ClO(<sup>2</sup>Π,  $\nu$ ), the nascent vibrational state distribution of ClO(<sup>2</sup>Π,  $\nu$ ), the quenching rate of ClO(<sup>2</sup>Π,  $\nu$ ) by other molecules in the atmosphere, and the rate and branching ratios of the O<sub>3</sub> + ClO(<sup>2</sup>Π,  $\nu$ ) reaction must all be measured.

The study of the effects of the medium on the photoreactivity of OCIO demonstrates that the reactivity and quantum yields for competing chemical processes can change dramatically. In particular, Cl production increases upon solvation and approaches unit efficiency (through generation of ClOO) in the matrix. These results

suggest additional photochemical mechanisms by which OCIO can contribute to O<sub>3</sub> depletion, should OCIO be adsorbed on or solvated within aerosols.

Work in progress (52) measures the sticking coefficients for OCIO on ice surfaces to obtain the OCIO content of atmospheric aerosols. Recent photochemical studies of OCIO in warm (80 to 150 K) ice matrices find quantitative conversion of OCIO to ClOO (53). Possible atmospheric consequences of OCIO in aerosols include vertical redistribution of Cl in the Antarctic vortex, release of active Cl by reaction with HCl, and heterogeneous photochemical O<sub>3</sub> depletion.

#### REFERENCES AND NOTES

- J. C. Farman, B. G. Gardiner, J. D. Shanklin, *Nature* **315**, 207 (1985).
- A. F. Tuck, T. R. Watson, E. P. Condon, J. J. Margitan, O. B. Toon, *J. Geophys. Res.* **94**, 11181 (1989).
- S. Solomon, *Nature* **347**, 347 (1990).
- World Meteorological Organization Report 20* (1990), vol. 1.
- J. G. Anderson, W. H. Brune, M. H. Proffitt, *J. Geophys. Res.* **94**, 11465 (1989).
- W. H. Brune, J. G. Anderson, K. R. Chan, *ibid.*, p. 16649.
- S. Solomon, R. W. Sanders, M. A. Carroll, A. L. Schmeltekopf, *ibid.*, p. 11393.
- C. Schiller *et al.*, *Geophys. Res. Lett.* **17**, 501 (1990).
- G. Brasseur and S. Solomon, *Aeronomy of the Middle Atmosphere* (Reidel, Dordrecht, Holland, 1986).
- S. Solomon, R. R. Garcia, F. S. Rowland, D. J. Wuebbles, *Nature* **321**, 755 (1986).
- M. A. Tolbert, *Science* **264**, 527 (1994).
- C. R. Webster *et al.*, *ibid.* **261**, 1130 (1993).
- D. R. Hanson and A. R. Ravishankara, *J. Geophys. Res.* **96**, 5081 (1991).
- M. J. Molina, T.-L. Tso, L. T. Molina, F. C.-Y. Wang, *Science* **238**, 1253 (1987).
- L. T. Molina and M. J. Molina, *J. Phys. Chem.* **91**, 433 (1987).
- S. P. Sander, R. R. Friedl, Y. L. Yung, *Science* **245**, 1095 (1989).
- M. B. McElroy, R. J. Salawitch, S. C. Wofsy, J. A. Logan, *Nature* **321**, 759 (1986).
- A. A. Turnipseed, J. W. Birks, J. G. Calvert, *J. Phys. Chem.* **95**, 4356 (1991).
- H. S. Muller and H. Willner, *Inorg. Chem.* **31**, 2527 (1992).
- V. Vaida, S. Solomon, E. C. Richard, E. Ruhl, A. Jefferson, *Nature* **342**, 405 (1989).
- K. A. Peterson and H.-J. Werner, *J. Chem. Phys.* **96**, 8948 (1992).
- S. Baer *et al.*, *ibid.* **95**, 6463 (1991).
- A. Arkel and I. Schwager, *J. Am. Chem. Soc.* **89**, 5999 (1967).
- F. J. Adrian, J. Bohandy, B. F. Kim, *J. Chem. Phys.* **85**, 2692 (1986).
- R. C. Dunn, B. N. Flanders, V. Vaida, J. D. Simon, *Spectrochim. Acta A* **48**, 1293 (1992).
- V. Vaida, K. Goudjil, J. D. Simon, B. N. Flanders, *J. Mol. Liq.* **61**, 133 (1994).
- R. C. Dunn and J. D. Simon, *J. Phys. Chem.*, in press.
- \_\_\_\_\_, *J. Am. Chem. Soc.* **114**, 4856 (1992).
- R. C. Dunn, J. Anderson, C. S. Foote, J. D. Simon, *ibid.* **115**, 5307 (1993).
- A. W. Richardson, R. W. Redding, J. C. D. Brand, *J. Mol. Spectrosc.* **29**, 93 (1973).
- K. Miyazaki, M. Tanoura, K. Tanaka, T. Tanaka, *ibid.* **116**, 435 (1986).
- C. Paillard, G. Dupre, H. AlAiteh, S. Youssefi-Stitou, *Ann. Phys. (Paris)* **14**, 641 (1989).
- J. L. Gole, *J. Phys. Chem.* **84**, 1333 (1980).
- J. A. Jafri, B. H. Lengsfeld III, C. W. Bauschlicher Jr., D. H. Phillips, *J. Chem. Phys.* **83**, 1693 (1985).
- E. C. Richard and V. Vaida, *ibid.* **94**, 153 (1991).

- \_\_\_\_\_, *ibid.*, p. 163.
- J. B. Coon, *ibid.* **14**, 665 (1946).
- S. Michielsen *et al.*, *ibid.* **74**, 3089 (1981).
- T. Baumert, J. L. Herek, A. H. Zewail, *ibid.* **99**, 4430 (1993).
- E. Ruhl, A. Jefferson, V. Vaida, *J. Phys. Chem.* **94**, 2990 (1990).
- E. Bishenden and D. J. Donaldson, *J. Chem. Phys.* **99**, 3129 (1993).
- H. F. Davis and Y. T. Lee, *J. Phys. Chem.* **96**, 5681 (1992).
- W. G. Lawrence, K. C. Clemitshaw, V. A. Apkarian, *J. Geophys. Res.* **95**, 18591 (1990).
- J. H. Glowina, J. Misewich, P. P. Sorokin, in *Supercontinuum Lasers*, R. R. Alfano, Ed. (Springer-Verlag, Berlin, 1990), pp. 1-4.
- A. J. Colussi, R. W. Redmond, J. C. Scaiano, *J. Phys. Chem.* **93**, 4783 (1989).
- A. J. Colussi, *ibid.* **94**, 8922 (1990).
- K. Johnsson, A. Engdahl, P. Ouis, B. Nelander, *J. Mol. Chem.* **293**, 137 (1993).
- \_\_\_\_\_, *J. Phys. Chem.* **96**, 5778 (1992).
- C. Reichardt, *Solvents and Solvent Effects in Organic Chemistry* (VCH, New York, 1988).
- R. L. Jones *et al.*, *J. Geophys. Res.* **94**, 11529 (1989).
- J. G. Anderson *et al.*, *ibid.*, p. 11480.
- C. J. Purcell, J. Conyers, P. Alapat, R. Parveen, *J. Phys. Chem.*, in press.
- J. T. Roberts, V. Vaida, L. A. Brown, J. D. Graham, in preparation.
- This work was supported by grants from the National Science Foundation (V.V., ATM-9222651, and J.D.S., CHE-9306485). We thank our co-workers on this project; R. C. Dunn, B. Flanders, C. Foote, J. L. Anderson, E. Richard, E. Ruhl, A. Jefferson, G. Frost, L. Brown, and S. Solomon. We also thank K. Peterson for many helpful discussions.

## RESEARCH ARTICLE

# Bent Helix Formation Between RNA Hairpins with Complementary Loops

John P. Marino, Razmic S. Gregorian Jr., Györgyi Csankovszki, Donald M. Crothers\*

The initial interaction between the ColE1 plasmid specific transcripts RNA I and RNA II, which function as antisense regulators of plasmid replication, comprises a transient complex between complementary loops found within the RNA secondary structures. Multidimensional heteronuclear magnetic resonance spectroscopy was used to characterize complexes formed between model RNA hairpins having seven nucleotide complementary loops. Seven base pairs are formed in the loop-loop helix, with continuous helical stacking of the loop residues on the 3' side of their helical stems. A sharp bend in the loop-loop helix, documented by gel electrophoresis, narrows the major groove and allows bridging of the phosphodiester backbones across the major groove in order to close the hairpin loops at their 5'-ends. The bend is further enhanced by the binding of Rom, a ColE1 encoded protein that regulates replication.

Regulation of the replication of the *Escherichia coli* plasmid ColE1 is mediated by the interaction of two plasmid encoded RNA transcripts, RNA I and RNA II, together with a plasmid encoded protein, Rom or Rop, which acts to control plasmid copy number (1). RNA I and RNA II interact initially by base-pairing between their complementary loop structures (2). Rom binds to the transiently formed intermediate complex, thus suppressing dissociation of the two RNAs and facilitating formation of a persistent hybrid duplex of the two RNAs (3), which in turn results in failure of replication initiation. The initial "kissing" (4)

interaction between complementary loops has been proposed as a structural motif of RNA interaction in other systems (5).

Studies of pairs of hairpins derived from the RNA I and RNA II transcripts demonstrated that the hairpins bind to each other solely through the interaction of their complementary loops, and that Rom specifically binds the structure formed by the interaction of these loops (6, 7). In addition, the stability of the complexes formed by these RNA hairpins varies in ways that do not correlate simply with the potential number and kind of Watson-Crick base pairs that could be formed between the complementary loops. The most striking example is the stability enhancement, 350 times greater relative to the wild type, observed for complexes formed between hairpins in which the wild-type loop sequences are inverted

J. P. Marino and R. S. Gregorian Jr. contributed equally to this work. All the authors are with the Department of Chemistry, Yale University, New Haven, CT 06511, USA.

\*To whom correspondence should be addressed.